Action of Taiwan Cobra Cardiotoxin on Membranes: Binding Modes of a β-Sheet Polypeptide with Phosphatidylcholine Bilayers[†]

Shih-Che Sue, P. K. Rajan, Ting-Shou Chen, Chang-Huain Hsieh, and Wen-guey Wu*

Department of Life Sciences, National Tsing Hua University, Hsinchu, Taiwan 30043

Received February 21, 1997; Revised Manuscript Received April 29, 1997[⊗]

ABSTRACT: The interaction of Taiwan cobra cardiotoxin (CTX A3), a basic polypeptide consisting of three-fingered loops and five-strand β-sheet structure, with zwitterionic dipalmitoylphosphatidylcholine (DPPC) has been studied by ^{31}P and ^{2}H NMR to understand the binding modes of CTX in membrane bilayers. The results, in conjunction with DPH fluorescence anisotropy and differential scanning calorimetry studies, show that CTX may penetrate and lyse the bilayers into small aggregates at a lipid/protein molar ratio of about 20 in the ripple $P_{\beta'}$ phase. Elevating the temperature to that of the liquid crystalline L_α phase leads to the fusion of the small aggregates into larger ones as evidenced by the change of the isotropic signal into a magnetically aligned ^{31}P signal with a marked reduction in the chemical shift anisotropy. ^{2}H NMR study on deuterium-labeled DPPC in the head group and fatty acyl region as a function of temperature and CTX concentration reveals a molecular model that CTX undergoes a redistribution between penetrating and peripheral binding states depending on the temperature studied. In addition, both the conformational and dynamic states of the phosphocholine head group of DPPC bilayers are significantly perturbed in the presence of CTX. Structural consideration of the CTX molecule indicates that the penetration binding mode of CTX with the DPPC bilayer may involve a novel membrane-binding motif identified recently in the three-fingered loops of P-type CTX. CTX can only bind to DPPC membrane peripherally in the L_α phase due to the mismatch of their hydrophobic lengths.

The three-fingered β-sheet cobra CTXs[1] exert a unique action on phospholipid membranes [for a recent review on CTX, see Wu (1997)]. Fluorescence and circular dichroism spectroscopic investigations of 10 different CTXs suggest that the two distinct types of CTXs, i.e., P- and S-type CTX, which contain Pro-31 and Ser-28 near the tip of loop 2, respectively, bind to phospholipid membranes by using different regions of the molecules (Chien et al., 1994). S-Type CTXs penetrate into the hydrophobic core of the membrane involving binding of loop 1 of the protein with the bilayer. Such a binding mode allows favorable electrostatic interaction between basic residues and the anionic lipid head group (Desormeaux et al., 1992) as also suggested by infrared spectroscopic characterization of CTX M2 (cardiotoxin IIa from Mozambique spitting cobra, *Naja mosambicca*). Solid state NMR studies suggest that from a mixture of phosphatidylglycerol (PG) and phosphatidylcholine (PC) CTX M2 segregates PG alone (Carbone & Macdonald, 1996) and disrupts completely the phosphatidic acid bilayer structure (Picard et al., 1996). CTX M2 also penetrates deep into the hydrophobic acyl chain and causes the formation of inverted micelles of cardiolipin (Batenburg et al., 1985; Batenburg & de Kruijff, 1988). Bougis et al. (1981) suggested, using monomolecular film technique, that S-type CTXs bind to anionic phospholipids via two distinct configurations, flat and edgewise. But, it has been observed that S-type CTXs do not bind to the zwitterionic PC membranes (Dufourcq et al., 1982).

In contrast, P-type CTXs bind to zwitterionic PC membranes stronger than S-type CTXs do because the former group contains an additional hydrophobic loop region (Chien et al., 1994). Recent high-resolution 2D NMR spectra of mixtures of toxin γ (from African black-necked spitting cobra, *Naja nigricolis*) with perdeuterated PC micelles show significant variation in the chemical shift of all three hydrophobic loops of CTX molecules (Dauplais et al., 1995). The chemical shift variation agrees with the X-ray crystal structure data of P-type CTXs, namely, toxin γ and CTX A5 (Chien et al., 1991), which show a continuous hydrophobic region formed by the three loops, about 34 Å long (Sun et al., 1997; Bilwes et al., 1994). Thus, the extended hydrophobic region of P-type CTX not only allows binding of the toxin to zwitterionic lipid but also facilitates penetration into the bilayers. The cytolytic effect of the toxin, also called cytotoxin, on many cell systems supports the above hypothesis. There is no spectroscopic evidence, however, to show that the β-sheet CTX generates a transmembrane element like that of other amphiphilic α-helix polypeptides such as melittin (Vogel, 1987; Pott & Dufourc, 1995), alamethicin (He et al., 1996; Mak & Webb, 1995), and magainin (Ludtke et al., 1996; Bechinger, 1996).

Numerous experiments show that basic α-helical amphiphilic polypeptides form an in-plane or transmembrane complex with phospholipid membranes depending on the

[†] This work was supported by the National Science Council, Taiwan (Grant 85-2113-M007-025Y).

* To whom correspondence should be addressed (fax, 886-35-715934; e-mail, lswwg@life.nthu.edu.tw).

[⊗] Abstract published in *Advance ACS Abstracts,* July 15, 1997.

[1] Abbreviations: CSA, chemical shift anisotropy CTX, cobra cardiotoxin; DPPC-d_4, deuterium-labeled DPPC at $C_\alpha D_2$ and $C_\beta D_2$ positions; DPPC-d_{62}, perdeuterated DPPC at both fatty acyl chains; DPH, 1,6-diphenyl-1,3,5-hexatriene; DPPC, dipalmitoylphosphatidylcholine; DSC, differential scanning calorimetry; FID, free induction decay; L_α phase, liquid crystalline phase; $L_{\beta'}$ phase, gel phase; $P_{\beta'}$ phase, ripple phase; LB, line broadening; NS, number of scans; PC, phosphatidylcholine; PG, phosphatidylglycerol; T_1, spin lattice relaxation time; T_p, pretransition; T_m, main transition.

S0006-2960(97)00413-3 CCC: $14.00

experimental conditions (Vogel, 1987; Weaver et al., 1992; Ludtke et al., 1996). Of particular relevance to the present study is the observation that melittin perturbs PC membrane and that melittin/PC complexes exhibit polymorphism as shown by solid state ^{2}H and ^{31}P NMR (Dufourc et al., 1986; Dempsey & Watts, 1987; Kuchinka & Seelig, 1989; Dempsey & Sternberg, 1991; Monette et al., 1993). By using fatty acyl chain-deuterated PC membranes, it has been shown that the location of melittin with respect to the bilayer seems to change with temperature. More interestingly, for peptide/lipid molar ratios, R_i, ranging from 1−2/100 to 10−20/100, melittin disrupts gel phase PC membrane in small discoidal objects if the samples have been incubated at temperatures between pre- (T_p) and main (T_m) lipid phase transition. Above T_m of the pure lipid, melittin induces formation of large vesicles which may be aligned and deformed under high magnetic field. The process appears to be inhibited by introducing cholesterol into the phospholipid bilayer (Pott & Dufourc, 1995). The extent of vesicle deformation under magnetic field has also been correlated with the extent of disk formation, but the mechanism responsible for the observed phenomenon remains a matter of discussion. It has been suggested that the fusion process occurring in the magnetic field, variation of membrane magnetic susceptibility, or modification of membrane elastic properties upon addition of melittin plays a role.

In this communication we show for the first time that the basic β-sheet polypeptide CTX A3, the major protein in Taiwan cobra venom containing 60 amino acid residues, behaves like the α-helix polypeptide melittin in interacting with phospholipid bilayers. CTX A3 induces the formation of small lipid aggregates, presumably discoidal micelles at the gel phase, and promotes fusion of the aggregates, which form extended bilayers at the main lipid phase transition temperature. These bilayers align magnetically like the melittin/PC complexes. The temperature dependence of the penetration of polypeptides in CTX/dipalmitoyl PC (DPPC) complexes is also shown by using ^{31}P and ^{2}H NMR spectroscopy. The magnetically induced alignment of PC bilayers further allows the detection of CTX free and CTX rich domains in PC bilayers in the gel state from the significant difference between the ^{31}P chemical shift anisotropy (CSA) values identifiable with such domains. It is suggested that β-sheet CTX may also undergo a structural transition between the in-plane and transmembrane forms depending on the physical state of lipid bilayers [see, for instance, Ludtke et al. (1996) and He et al. (1996)].

MATERIALS AND METHODS

Purification of CTX. CTX A3 from *Naja atra* snake venom (Sigma Chemical Co., St. Louis, MO) was purified by SP-Sephadex C-25 ion exchange column chromatography as reported (Chien et. al., 1991; 1994). The purity of CTX preparations as tested by SDS−polyacrylamide gel electrophoresis and analytical reverse phase high-performance liquid chromatography (HPLC) was found to be higher than 99%. Lyophilized CTX obtained directly from HPLC was found to degrade phospholipids during NMR experiments. Therefore the phospholipase A2 activity was abolished using the well-established technique by chemically modifying the histidine residue of the enzyme with *p*-bromophenacyl bromide and adding EDTA to the sample (Abe et al., 1977). It was observed that such a treatment, however, could not prevent the degradation effect if the sample was incubated for a long time (>2 days). It was found that some residual acidic component was still present after HPLC, and thus the CTX was purified further by extensive dialysis of the toxin with distilled water. No degradation was observed in the phospholipids after these extensive purification steps. As an additional precaution, the samples used in the NMR experiments were checked through thin layer chromatography before and after the experiments, and we could confirm that there were no sample degradations. The NMR data collection was performed within 24 h after a given sample was prepared freshly. Moreover, if degradation were to be present, it would have reflected as an anomalous increase in the main transition temperature (Dempsey & Watts, 1987), and this was not observed in our case.

Preparation of CTX/DPPC Samples. The lipids used in this work, namely, pure dipalmitoylphosphatidylcholine (DPPC) as well as acyl chain-perdeuterated DPPC (DPPC-d_{62}) and head group-labeled DPPC (DPPC-d_4) were obtained commercially (Avanti Polar Lipids, Alabaster, AL). Deuterium-depleted H_2O was purchased from Cambridge Isotope Laboratory (Woburn, MA). All the samples were prepared in fully hydrated conditions (∼80 water molecules/DPPC) in preweighed NMR tubes, using a known amount of phospholipid and purified CTX where necessary.

Samples used for observation without thermal cycling were prepared in the following way. Weighed lipid samples in the NMR tubes were evacuated for at least 6 h, and a solution of deuterium-depleted H_2O and EDTA (10 mM) with the appropriate stoichiometric quantity of CTX was added to the evacuated lipid at ambient temperature well below the pretransition temperature of 35 °C. CTX/DPPC dispersion was then agitated mechanically to ensure the homogeneity of the sample. The pH of the samples was brought to 6.5, and the tubes were sealed using septa.

For the experiments requiring thorough freeze−thaw, the following procedure was used. First the sample was prepared by the above-mentioned procedure, and it was incubated in an oven 5−10 °C above the gel to liquid crystalline transition temperature (41 °C) for 10 min. The temperature of the sample was then brought back to 4 °C in a freezer. This cycle was repeated at least five to six times to ensure complete homogeneity of the CTX/DPPC complex. The thus homogenized sample was sealed with septa. The pretransition as well as gel to liquid crystalline phase transition temperatures of DPPC-d_{62} were found to shift by 4 °C below those of pure DPPC. For uniformity the transition temperatures in this work are denoted by T_p (pretransition) and T_m (main transition), irrespective of the type of DPPC.

NMR Data Acquisition and Line Shape Simulation. ^{2}H and ^{31}P NMR spectra were obtained on a 7.05 T Bruker MSL-300 spectrometer (Germany) using a broad-band probe horizontally mounted with a 5 mm insert (Hsieh & Wu, 1996). ^{31}P NMR spectra were recorded with Hahn echo pulse sequence using a 90° pulse of 4 μs with ^{1}H decoupling and an interpulse delay of 20 μs. The repetition time of the pulse sequence was 7 s. ^{2}H NMR spectra were recorded with a quadrupole echo pulse sequence ($90°_x-\tau-90°_y-\tau-$FID) using 90° pulses of ∼2.6 μs duration (depending on the temperatures). The interpulse delay τ was 20 μs, and the maximum recycle delay used was 1 s. Spin−lattice relaxation time (T_1) was measured using inversion recovery sequence ($180°_x-\tau-90°_x-$FID). Recycle delays were longer

than $5T_1$, ranging from 150 ms to 2 s in the entire temperature range covered for ^{31}P and ^{2}H NMR spectra. The dwell time used to obtain the spectra was typically ~4.0 μs. For all the ^{31}P NMR spectra, a line broadening (LB) of 50 Hz was used, unless otherwise specified. For the ^{2}H NMR spectra the LB used was 20 Hz for all the spectra. The temperature of the samples studied was controlled either by evaporation of N_2 from a liquid nitrogen Dewar for low-temperature measurements or by the flow of heated dry air for high temperatures and in both cases was monitored by a Bruker VT-1000 thermal system to an accuracy of ±1 °C. The CSA values of all ^{31}P NMR spectra were referenced with respect to the PO_4 resonance of H_3PO_4, which is taken to be 0 ppm.

The individual resonances from different species of deuterium in the ^{2}H NMR powder spectra were extracted by using the numerical dePakeing technique (Bloom et al., 1981; Sternin et al., 1983). The segmental order parameters for different carbon atoms on the acyl chain were calculated from the dePaked spectra, and these were used to compute the hydrophobic thickness as well as the average area of cross sections of the acyl chain region of DPPC (Seelig & Seelig, 1974; Schindler & Seelig, 1975; Salmon et al., 1987). The ^{2}H NMR powder spectra were simulated using the Pake formula for a random dispersion of the bilayers with the distribution of intensities of individual resonances taken from the dePaked spectra (Pake, 1948; Schmidt-Rohr & Spiess, 1994; Davis, 1979). It has been shown that bilayers which are oriented by the effect of the magnetic field have an ellipsoidal distribution of the bilayer normals (Pott & Dufourc, 1995). For the simulation of ^{2}H NMR powder spectra aligned in the magnetic field, such an ellipsoidal distribution was used in place of the spherical distribution (Schmidt-Rohr & Spiess, 1994).

DSC and Fluorescence Anisotropy Measurements. DSC measurements were made on a SEIKO model DSC-100 differential scanning thermal system. Heating runs of the samples from the gel state were recorded at a heating rate of 1 °C/min. The fluorescence anisotropy measurements were carried out on an SLM 4800 spectrofluorometer. DPH (1,6-diphenyl-1,3,5-hexatriene) molecules, embedded in the acyl chain region of the lipid dispersion, at a molar ratio of 0.1%, were used as the probe for the fluorescence measurements. The DPH containing sample was excited at 360 nm, and the emission intensity was recorded at 431 nm by using a filter to cut off wavelengths below 389 nm. The recorded intensities were used to compute the fluorescence anisotropy r (Wu & Huang, 1983) given by

$$r = (I_{=} - I_{\perp})/(I_{=} + 2I_{\perp})$$

where $I_{=}$ and $I_{\perp}$ represent the emission intensity parallel and perpendicular, respectively, to the plane of polarization of the excitation beam. The temperature of the sample in the cuvette holder was controlled within 0.2 °C by a refrigerated water bath circulator (Neslab RTE-4) equipped with a digital temperature controller (Neslab DCR-1).

RESULTS

^{31}P NMR. ^{31}P NMR spectroscopy is popular to study discoidal micellization and magnetically induced orientation effected by amphiphilic polypeptides in PC membranes (Monette et al., 1993; Qiu et al., 1993; Pott & Dufourc, 1995). ^{31}P NMR is well suited to study conformational and dynamic changes specifically from the head group regions in PC membranes. Unoriented liposomes normally exhibit axially symmetric ^{31}P powder patterns (Figure 1A) with resonances distributed between $\sigma_{\perp}$ and $\sigma_{=}$, reflecting the chemical shift dependence on the molecular orientation with respect to the magnetic field (Smith & Ekiel, 1984). When the size of these liposomes becomes comparable to or smaller than that of micelles or sonicated vesicles, say, due to a strong interaction with a molecule like CTX, they tumble freely and the isotropic reorientation of such aggregates will show up as a single line at 0 ppm in the spectrum (for instance, see the trace obtained at 39 °C in Figure 1B). On the other hand, for a completely oriented lipid at 90° relative to the applied field, i.e., when the phospholipid membrane plane becomes parallel to the magnetic field, the axially symmetric powder pattern collapses to a single resonance centered at $\sigma_{\perp}$ (see, for instance, the trace obtained at 45 °C in Figure 1B). In the present study, such unique signatures in the ^{31}P NMR spectra are effectively utilized to characterize the effect of CTX on the macroscopic organization of DPPC membranes and the extent of interaction of CTX with bilayers upon thermal cycling of the CTX/DPPC complexes.

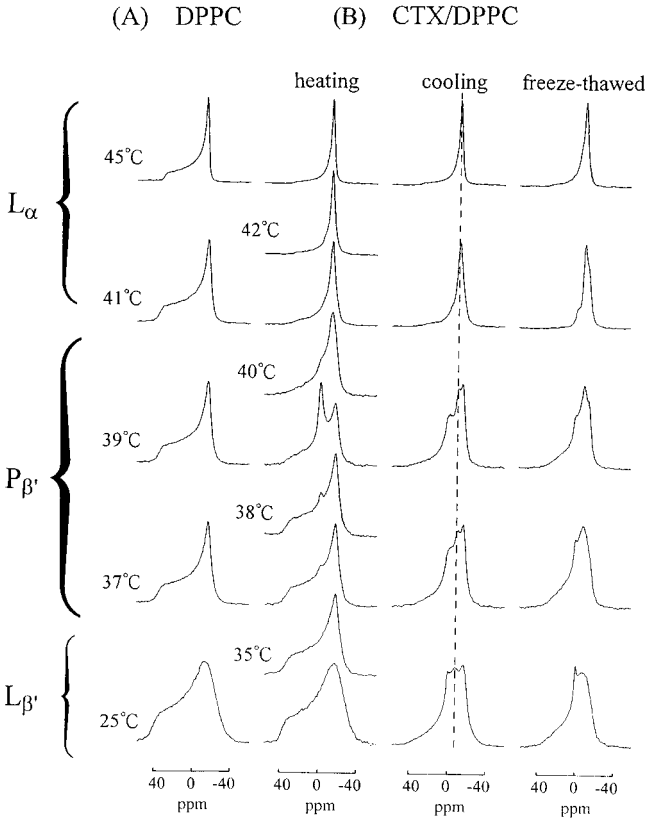

FIGURE 1: ^{31}P NMR spectra as a function of temperature from CTX/DPPC complexes in a molar ratio 3/200. LB is 50 Hz for all the ^{31}P NMR spectra, unless otherwise specified. NS varies from 400 in gel state to 300 scans in L_α phase. (A) Control spectra of DPPC without CTX. (B) Spectra from the CTX/DPPC complex during the first heating scan from the gel $L_{\beta'}$ state (left panel), during the first cooling scan from the liquid crystalline L_α state (middle), and during the heating scan after several cycles of freeze and thaw (right). Pretransition temperature (T_p) is 35 °C, and main transition temperature (T_m) is 41 °C for DPPC.

The history dependence of the effect of CTX A3 on DPPC bilayers at R_i of 3/200 was investigated first, because amphiphilic polypeptides of melittin do not perturb the DPPC bilayer at the gel state unless the complexes are incubated

at temperatures higher than T_p or T_m. Figure 1B shows the ^{31}P NMR spectra obtained during the heating scan. These spectra appear to be similar to those of pure DPPC (Figure 1A) at the $L_{\beta'}$ phase until the temperature reaches the pretransition temperature T_p at about 37 °C. A significant isotropic signal centered at 0 ppm becomes apparent at temperatures above T_p but disappears as the temperature reaches the main transition temperature of T_m , viz., 41 °C. We observed that this isotropic signal during the first heating scan is completely reproducible every time, when the sample is freshly prepared and heated from the gel state through the ripple phase. We also observed that, as the sample is heated from the gel state, it changes from a milky white to transparent fluid and turns turbid again as it changes into the liquid crystalline phase. From these observations we conclude that the solubilization of DPPC membranes by CTX to become small phospholipid aggregates appears to occur in the ripple $P_{\beta'}$ phase, a phenomenon similar to the action of melittin on DPPC−cholesterol dispersions (Pott & Dufourc, 1995). Picard et al. and Batenburg et al. had earlier observed isotropic signals in ^{31}P NMR spectra in their studies of DMPA/CTX and cardiolipin/CTX complexes. In these cases, it has been suggested that formation of inverted micelles leads to such an observation. The data presented here are distinctly different in the following respects. The ^2H NMR data from the perdeuterated acyl chain region (see section on ^2H NMR results) in the present case clearly rule out the possibility of inverted micelle formation. Further, in the case of CTX interaction with cardiolipin and DMPA, the inverted micelle formation is triggered by the strong attractive force of the negatively charged lipid toward the positively charged S-type CTX where the primary site of interaction between the lipid and CTX is the head group region, whereas in the case of CTX A3, the primary region of interaction is the hydrophobic acyl chain portion of the lipid with the hydrophobic region of CTX, and the favorable bilayer thickness aids in the penetration and sustenance of the β-sheet CTX A3 in the transmembrane conformation, leaving the lamellar structure intact, as seen from the data presented later.

At temperatures above T_m, the symmetric powder pattern of ^{31}P NMR spectra with a CSA value similar to that obtained from pure PC membranes (compare parts B and A in Figure 1) becomes centered near the resonance at $\sigma_\perp$. This change is perhaps due to the magnetic alignment of DPPC bilayers parallel to the magnetic field. More strikingly, the appearance of the aligned bilayers coincides with the disappearance of small DPPC aggregates, as seen from the absence of the isotropic line from these spectra. One possible explanation is that the isotropic ^{31}P signal may also represent discoidal micelles similar to the ones found in the melittin/DPPC complexes and such discoidal micelles fuse to form extended bilayers at T_m.

The ^{31}P NMR spectra obtained during cooling at temperatures below T_m are distinctly different from those obtained during the first heating scan beginning from the gel phase (compare middle panel with left panel of Figure 1B). The CSA is smaller, and there are at least three components, indicating the occurrence of irreversible phase segregation in the gel state. In fact, the three components in the ^{31}P NMR spectra found in the cooling scan are still present for the samples after extensive freeze−thaw representing the equilibrium state of the CTX/DPPC complex, though their respective intensities are different from the three components observed during the first cooling scan (right panel of Figure 1B). In Figure 1B, therefore, the isotropic signal indicates the presence of only the discoidal micelles rich in CTX and at a concentration of 3/200 CTX does not seem to completely lyse all the bilayers into discoids as evidenced from the presence of a broader component with a CSA of 47 ppm, and this component should correspond to the predominantly CTX free bilayer dispersions. The third component with a CSA of about 40 ppm perhaps represents an intermediate state where the CTX molecules in the transmembrane configuration may induce the lysed discoids to fuse edgewise into larger aggregates which are less susceptible to motional averaging thereby rendering a line in between the isotropic signal and the broad component. Nevertheless, at this stage it is difficult to confirm whether such a fusion process is a dynamic and reversible one or not.

The three different components in the spectra seen in the ripple $P_{\beta'}$ phase from samples subjected to thorough freeze−thaw are not distinctly identifiable in the liquid crystalline L_α phase. The situation is more complex in the liquid crystalline phase, but one possible interpretation of the spectrum in the L_α phase is that the smaller discoids fuse together to form stable large aggregates which are magnetically aligned, with the bilayer normals being perpendicular to the magnetic field. Such a fusion will be encouraged by any possible mismatch in the hydrophobic thickness of the bilayer in the L_α phase with that of the CTX molecule, as demonstrated later (see section on ^2H NMR data). The magnetically induced alignment of the fused discoids rich in CTX molecules may persuade the CTX free bilayer dispersions also to partially orient in the magnetic field. In such a case, there will no longer be any isotropic signal in the ^{31}P NMR spectrum, and one can expect a component from an oriented bilayer superposed onto a partially aligned powder spectrum, which is indeed what is observed in the L_α phase.

Since CTX is observed to interact with DPPC strongly in the ripple phase, the study was extended to look at the dependence of the CTX binding mode with DPPC on the concentration of CTX. Experiments were performed as a function of CTX/DPPC molar ratio at the temperature of ripple phase formation, and the spectra are shown in Figure 2. The representative traces of ^{31}P NMR spectra show that increasing the amount of CTX causes the appearance of an isotropic ^{31}P signal with an increasing intensity in the studied temperature range of a few degrees below T_m. Complete disruption of the anisotropic bilayer signals in the ripple phase occurs when the CTX to DPPC molar ratio is ∼5/100. Therefore, all the isotropic NMR signals shown in Figure 1 indeed represent those from CTX rich DPPC discoidal micelles.

DSC and Fluorescence Anisotropy. We performed DSC measurements to confirm the apparent phase segregation of CTX/DPPC complexes as suggested by ^{31}P NMR. As shown in Figure 3B, an initial heating scan of the CTX/DPPC complex reveals a small endothermic peak around 39 °C just before the main DPPC transition at T_m (Figure 3A). After the samples were frozen and thawed several times, this endothermic peak grew in intensity. This rise suggests that the freezing and thawing process may promote the interaction between CTX and DPPC membranes and increase the apparent population of the equilibrium CTX/DPPC complex.

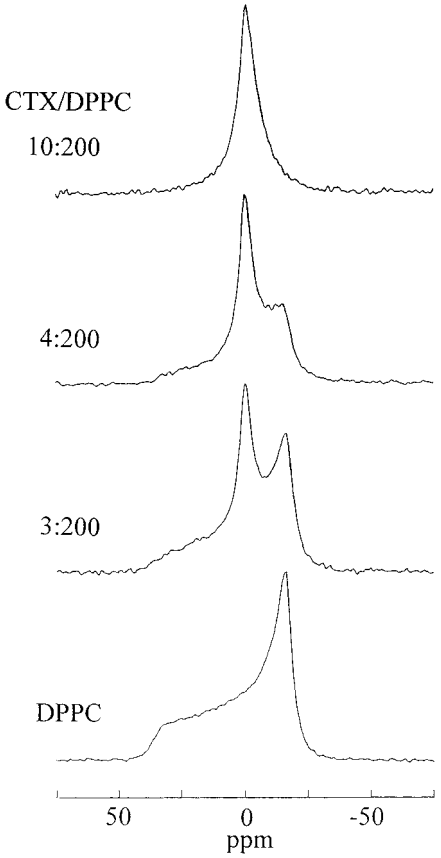

FIGURE 2: Variation of ^{31}P NMR spectra as a function of increasing CTX concentration. Molar ratios of CTX to DPPC are adjacent to the spectra. The temperatures of the sample are 2 °C below T_m. Spectra were recorded during the first heating scan from the gel phase. Note the complete absence of a powder-like spectrum at molar ratio 5%.

The molecular composition of the CTX/DPPC complexes thus formed can be estimated by calculating the molar ratio of the sample giving only the endothermic transition around 39 °C. This estimate indicates that about 5 mol % CTX is adequate to erase the pure DPPC endothermic transition at 41 °C (inset panel in Figure 4). In this limit, it can be estimated that the segregated CTX/DPPC complex contains about 20 DPPC molecules/CTX molecule. A similar conclusion can also be made based on the effect of the CTX concentration on the CSA of ^{31}P NMR spectra obtained at the liquid crystalline L_α phase (Figure 4). The CTX concentration dependent plot of the CSA of the ^{31}P signal also seems to saturate around 5 mol % of CTX in DPPC.

Additional evidence to indicate the importance of ripple phase formation in inducing the lytic activity of CTX toward DPPC membranes can be found in DPH fluorescence anisotropy measurements on CTX/DPPC complexes. The fluorescence anisotropy as a function of temperature for pure DPPC with a DPH probe is presented along with the DSC data. Figure 3B (bottom panel) shows the fluorescence anisotropy of a CTX/DPPC suspension (3/200) when the sample was scanned from the temperature of the gel phase into the liquid crystalline phase and also after the sample was run through several freeze−thaw cycles. When the CTX/DPPC complex passes through the pretransition temperature T_p in the first heating scan, the anisotropy increases perceptibly. After several freeze−thaw cycles the anisotropy reaches an equilibrium value similar to that of pure DPPC. The reason for the much lower anisotropy value of DPH in

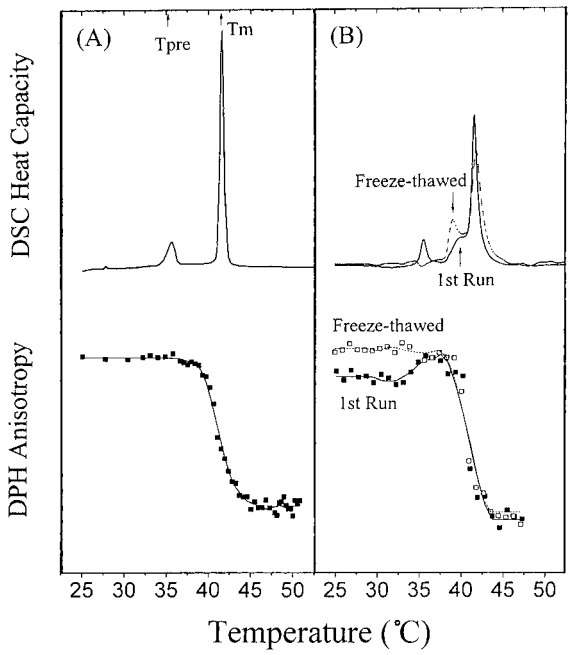

FIGURE 3: DSC heat capacity and fluorescence anisotropy variation as a function of temperature for pure DPPC and the CTX/DPPC complex at molar ratio of 3/200: (A) control data from pure DPPC obtained in the heating scan and (B) traces obtained during the heating scans in the first run and after extensive freeze−thaw through T_m. Continuous and dotted lines show the variation for the first heating scan and after several freeze−thaw cycles, respectively.

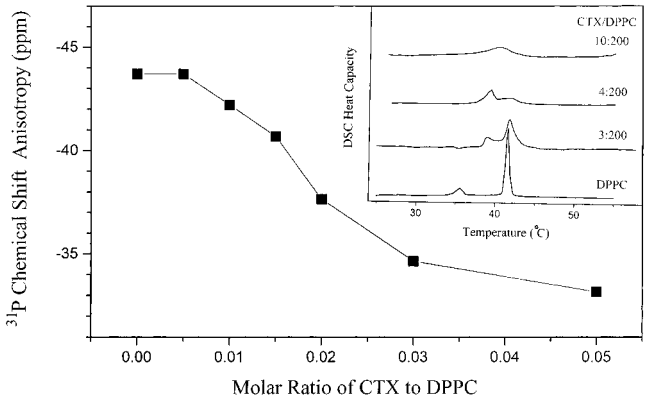

FIGURE 4: Dependence of ^{31}P chemical shift anisotropy (CSA) and endothermic heat capacity as a function of CTX concentration in DPPC. The CSA values were obtained in the L_α phase. The solid line is to guide the eye. The saturating effect of 5 mol % CTX in DPPC is clearly seen. Inset figure shows the respective DSC heat capacity traces at different CTX concentrations, demonstrating the strong effect of CTX on DPPC erasing the endothermic transition of pure DPPC to become a broad transition of the CTX/DPPC complex at slightly lower temperature.

the initial run is unclear at present. It may reflect a complex interaction between DPH and two other studied molecules of a CTX/DPPC dispersion. Although the details of the mechanism are unclear, the result corroborates the ^{31}P NMR data that CTX interacts with DPPC in the $P_{\beta'}$ phase, as seen during the first heating scan from the gel state.

^{2}H NMR. In order to examine how CTX perturbs PC bilayers, experiments were also performed using perdeuterated DPPC (DPPC-d_{62}). The aim was also to look for possible effects on the packing and ordering of the hydrophobic region of the bilayer within the CTX/DPPC complex which will provide us with additional insight into the binding

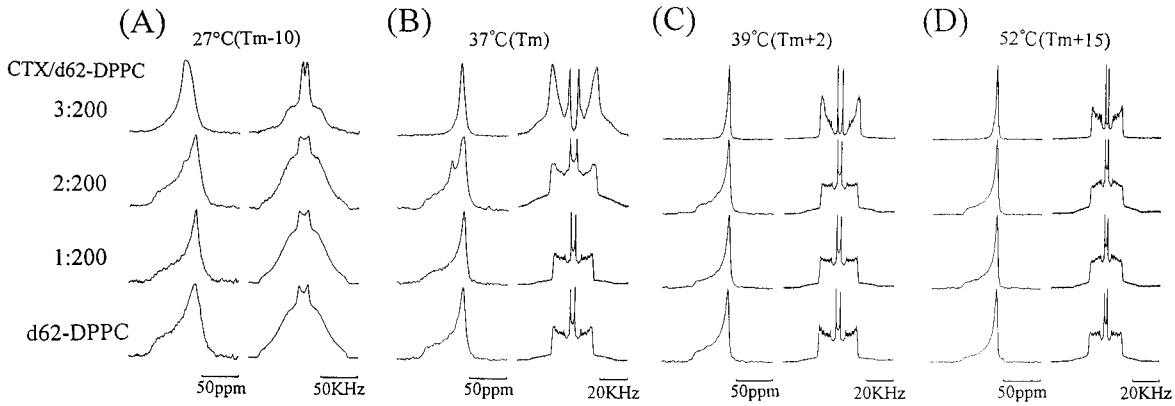

FIGURE 5: Traces of ^{2}H and ^{31}P NMR spectra showing the effect of variation of CTX concentration at different temperatures. LB used for all ^{2}H NMR spectra is 20 Hz, unless otherwise specified. The last (bottom) row in all the panels shows control spectra from DPPC-d_{62} without CTX. The three different concentrations of CTX used are indicated at the left of panel A. Note that the T_m of DPPC-d_{62} is about 4 °C lower than that of undeuterated DPPC.

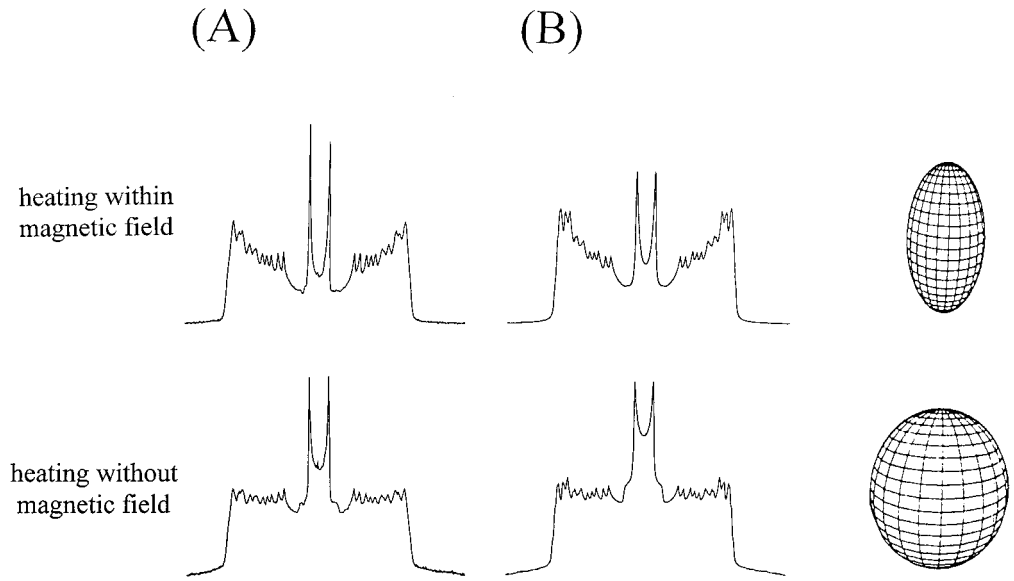

FIGURE 6: Demonstration of the alignment of fused bilayer aggregates in the presence of a strong magnetic field. (A) Spectra obtained from the CTX/DPPC-d_{62} complex (4/200 molar ratio) heated to the L_α phase in the presence of a magnetic field (top) and in the absence of a magnetic field (bottom). (B) Computer-simulated spectra, considering the bilayer-aligning effect of the magnetic field (top) and the conventional powder-like distribution of bilayers (bottom). See Materials and Methods in the text for details.

modes of CTX and bilayers. Figure 5 shows the ^{2}H NMR spectra of the acyl chain-perdeuterated DPPC in the presence of different concentrations of CTX at different temperatures. The ^{31}P NMR spectra are also provided for comparison. It should be noted that these spectra were obtained after several freeze−thaw cycles of the samples. The ^{31}P NMR spectra were obtained from the perdeuterated samples. At (T_m − 10) °C, the ^{2}H NMR spectrum obtained is characteristic of the gel state of pure DPPC at a low CTX/DPPC ratio (see Figure 5A) (Davis, 1979). As the concentration of CTX increases not only the CSA of the ^{31}P signal but also the apparent quadrupolar splittings of the ^{2}H signal show a significant reduction. In the liquid crystalline state, high CTX content produces magnetically aligned ^{31}P NMR spectra with slightly reduced CSA (left columns in Figure 5C,D). The effect of CTX on the ^{2}H NMR spectra in the liquid crystalline state is complex. Both the line shape (see the three upper traces of the ^{2}H signal and also the ^{2}H traces as a function of concentration in Figure 5B−D) and the quadrupole splittings are different from pure DPPC-d_{62}.

The lower signal intensity for ^{2}H NMR frequencies distributed near the center of the spectra at temperatures just above T_m can be understood to be a result of magnetically induced orientation of the membrane bilayer, suggested previously based on the ^{31}P NMR data. Such an alignment effect induced by the magnetic field can best be demonstrated by first taking the CTX/DPPC complex into the L_α phase from the $P_{\beta'}$ phase in the presence of the magnetic field and recording the spectra and in a second case heating the sample into the liquid crystalline phase from the gel state in the absence of the magnetic field and recording the spectra again. The comparison of the two spectra will clearly reveal the alignment effect. The top and bottom panels of Figure 6A show the spectra recorded from the CTX/DPPC complex following such a procedure, and the effect of the magnetic field is clearly seen. To corroborate the alignment effect further, we performed computer simulation of the spectra. The bottom panel of Figure 6B shows the computer-simulated powder pattern by considering a conventional distribution of bilayers oriented randomly in all directions (Davis, 1979; Schmidt-Rohr & Spiess, 1994). The top panel of Figure 6B shows the simulated ^{2}H NMR spectrum for bilayers oriented in the magnetic field with the bilayer normals following an ellipsoidal distribution in space (Pott

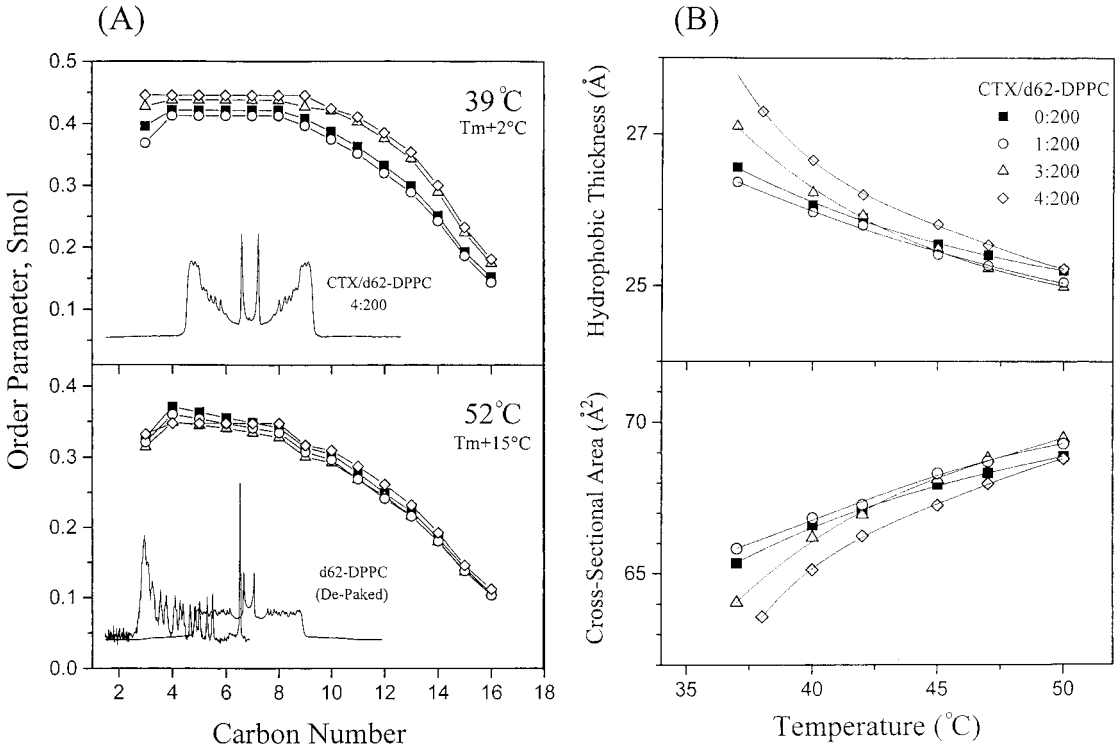

FIGURE 7: (A) Segmental order parameter S_{mol} at the respective carbon atoms counted from the head group end of the DPPC-d_{62} molecule. Top panel shows the order parameter change as a function of CTX concentration at (T_m + 2) °C. Bottom panel shows the variation well inside the L_α phase. Representative oriented and dePaked ^{2}H NMR spectra are also shown. (B) Hydrophobic thickness (top) and cross sectional area of the acyl chain region (bottom) at three different CTX concentrations calculated based on Salmon et al. (1987). See the text for more details.

& Dufourc, 1995; Schmidt-Rohr & Spiess, 1994). On the basis of the similarity between the experimental and theoretical ^{2}H NMR spectra, we conclude that the DPPC dispersion orients partially during the fusion process of the putative discoidal micelles. The magnetically oriented DPPC bilayers, however, become less apparent at higher temperature due probably to the thermally induced agitation of the dispersion (Figure 5). It should be noted that magnetically induced orientation of CTX/DPPC complexes does not produce any change in the quadrupolar splittings. This was verified by comparing the $\Delta\nu_Q$ of the individual resonances from both magnetically aligned and unoriented powder patterns using the dePakeing technique. It is to be emphasized that we have also observed magnetically oriented ^{31}P NMR spectra similar to the present case for sphingomyelin/CTX complexes (data not shown), confirming that the observed oriented spectra in the present case are not due to sample degradation by PLA2 activity, as PLA2 does not target sphingomyelin.

As we have taken into account the magnetic alignment of the bilayer to explain the distorted NMR powder spectra near T_m, the effect of CTX on the fatty acyl chain packing of DPPC can now be examined quantitatively (Figure 7A). Quantitative analysis of the order parameter profile of DPPC-d_{62} by applying the dePakeing technique suggests that CTX perturbs the fatty acyl chain packing of the DPPC bilayer interestingly. At temperatures far above T_m, for instance at 52 °C, increasing CTX concentration reduces the order parameter profile of the DPPC bilayer (bottom frame of Figure 7A). In contrast, at a temperature just above T_m , for instance at (T_m + 2) °C, the effect of increasing CTX concentration does not appear to be linear. Though this effect is small when the inevitable minimum error in the calculation of the segmental order parameters is taken into account, it is clearly seen that the penetration of β-sheet CTX affects the overall order of the acyl chain region in a perceptible way (Figure 7A). It is interesting to point out that high concentration of CTX reduces the molecular order in the head group region, as indicated by the reduced CSA of the ^{31}P signal and the quadrupolar splitting of the ^{2}H signal in the head group region (see Figures 5 and 9).

To understand the physical nature of this effect, we converted these data into molecular parameters of DPPC bilayers (Figure 7B) since the order parameter profiles obtained by ^{2}H NMR are suggested to provide useful information on the hydrophobic thickness and cross sectional area of the studied lipid (Salmon et al., 1987). At temperatures right above T_m, the estimated bilayer thickness of CTX/DPPC appears to be larger than that of pure DPPC. The average cross sectional area per lipid in the acyl chain region just above T_m is smaller for the CTX/DPPC complex compared to that of pure DPPC. These observations imply that the lipid molecules are rather closely packed in the presence of CTX around T_m when the CTX molecules are anchored within the hydrophobic core of the bilayers which is also consistent with the ^{31}P NMR data.

We were unable to resolve ^{2}H NMR signals from the two coexisting phases as detected in ^{31}P NMR spectra and DSC results. In particular, the characteristic isotropic line, representative of the lysed discoids detected in the ripple phase, observed in the ^{31}P NMR spectra is also absent in the ^{2}H NMR spectra from the tail region. It should be emphasized that the possibility of short recycle delays diminishing the signal intensity of such a line is ruled out in our case by keeping the recycling delays well above $5T_1$. To shed more light on this problem, we also collected ^{2}H

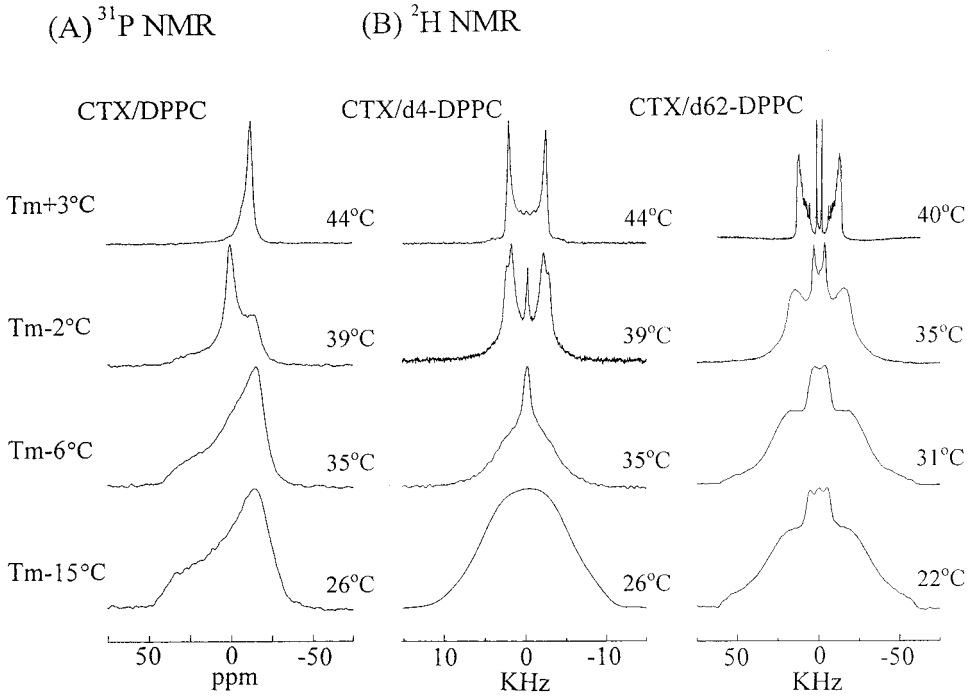

FIGURE 8: Effect of CTX on the NMR spectra representing the conformational and aggregating property of the CTX/DPPC complex in the head group and fatty acyl chain regions: (A) ^{31}P NMR spectra showing the lysing action of CTX in the ripple $P_{\beta'}$ phase [middle panel at (T_m − 2) °C] and the aligned bilayer aggregates in the liquid crystalline L_α phase (top panel) and (B) ^{2}H NMR spectra from head group-labeled DPPC with the isotropic line from small aggregates in the $P_{\beta'}$ phase (left) and ^{2}H NMR spectra from the acyl chain region of DPPC with no detectable isotropic signal (right). All the spectra were recorded in the first heating run from the $L_{\beta'}$ phase. See the text for the interpretation.

NMR spectra from the head group region by using DPPC-d_4 bilayers selectively deuterated in the head group region at the C_α and C_β positions. Figure 8 shows the respective ^{31}P and ^{2}H NMR spectra of the CTX/DPPC complex at a molar ratio of 4/200. The left panel of Figure 8B shows the ^{2}H NMR spectra obtained exclusively from the head group region, and the right panel shows those from the tail region. The spectra in this figure correspond to the sample incubated in the gel state and taken from the gel state to the liquid crystalline state for the first time. The spectrum from the head group, when the sample is well into the gel state at a temperature of (T_m − 15) °C, is a broad line similar to that observed for pure DPPC. When the sample was heated into the ripple phase [spectra at (T_m − 6) and (T_m − 2) °C] a clear isotropic line is seen overlapping with the familiar Pake pattern. Macdonald et al. (1991) had earlier demonstrated that well-resolved quadrupolar splittings of NMR spectra can be detected for DPPC-d_4 in the ripple phase.

When the temperature of the sample is increased to that of the L_α phase, the isotropic line disappears. These data, along with ^{31}P NMR spectra (Figure1), therefore confirm the formation of the tiny discoids owing to the strong interaction of CTX with the DPPC bilayers. Comparison of the data from the head group and tail regions of the lipid molecules supports the possibility that the conformational state and the dynamic changes taking place at the head group region are not necessarily similar to those at the tail region which is consistent with the absence of an isotropic line from the tail region data in contrast to the clear appearance of the same in the head group data.

Figure 9 presents the ^{2}H NMR spectra of DPPC-d_4 with CTX at three different temperatures after the sample was subjected to many freeze−thaw cycles. The bottom panel shows the spectra of DPPC-d_4 without CTX, at just above the gel to ripple transition temperature (37 °C), a few degrees above the main transition into the L_α phase (44 °C) and well into the liquid crystalline phase (52 °C). The top panel shows the spectra from the CTX/DPPC complex at the same temperatures. The spectrum of the CTX/DPPC complex at 37 °C shows clearly resolved lines from the two different sets of deuterium nuclei at the C_α and C_β positions. The lines from two different sets of deuterium at the C_α and C_β positions merge together at 44 °C and once again appear resolved at 52 °C. The change in the quadrupole splitting as a function of temperature in this fashion points to a possible change in the head group conformation.

Our assignment of the two different sets of resolved Pake doublets to the C_α and C_β positions is based on the relaxation behavior of the two signals since selectively deuterated DPPC at only one site like C_α or C_β was unavailable for this study. To help assign the peaks to appropriate positions, T_1 relaxation time measurements were performed and are reported at two representative temperatures as shown in Figure 10A. It is established that the deuteron labeled at the β-position exhibits larger T_1 due to the faster motion of $C_\beta D_2$ than $C_\alpha D_2$ (Pinheiro et al., 1994) and that the T_1 temperature dependent profile is in the fast motional regime. Based on this observation, the $\Delta\nu_Q$ of DPPC-d_4 is seen to decrease and increase for $C_\beta D_2$ and $C_\alpha D_2$, respectively (Figure 10B). This is in sharp contrast to the variation of the quadrupole splitting of pure DPPC-d_4 as a function of temperature, showing a continuous decrease for both deuterated positions. According to the choline tilt model (Roux et al., 1989; Macdonald et al., 1991), the opposite behavior of the quadrupolar splitting of two NMR signals in the CTX/DPPC-d_4 complex suggests that the P−N dipole of the PC head group tilts toward the water phase in the ripple phase but may swing back to the normal head group orientation in

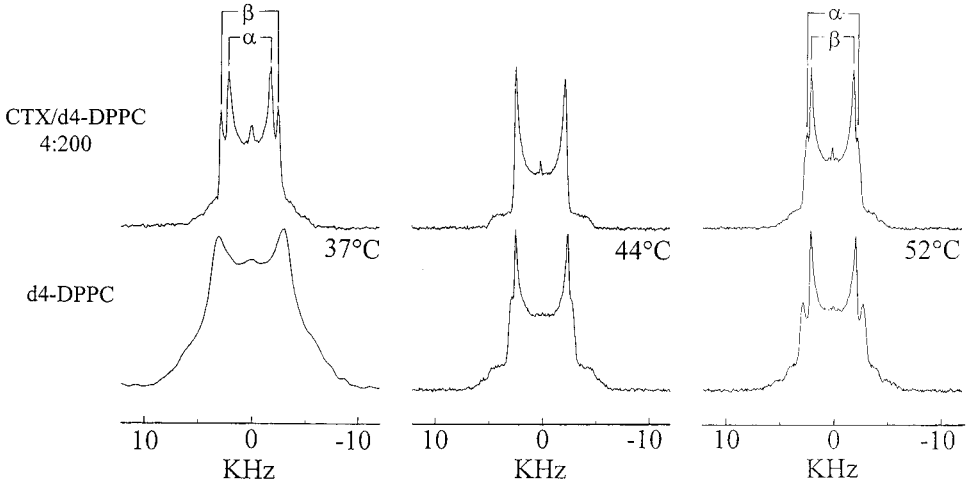

FIGURE 9: ^{2}H NMR spectra of the head group region of the CTX/DPPC-d_4 complex (4/200 molar ratio) at three different temperatures. Samples were thoroughly homogenized by subjecting to several cycles of freeze and thaw. Bottom panel shows the control spectra from DPPC-d_4. Assignments of ^{2}H belonging to C_α and C_β carbons are marked on the spectra. Refer to Figure 10 and the text for details.

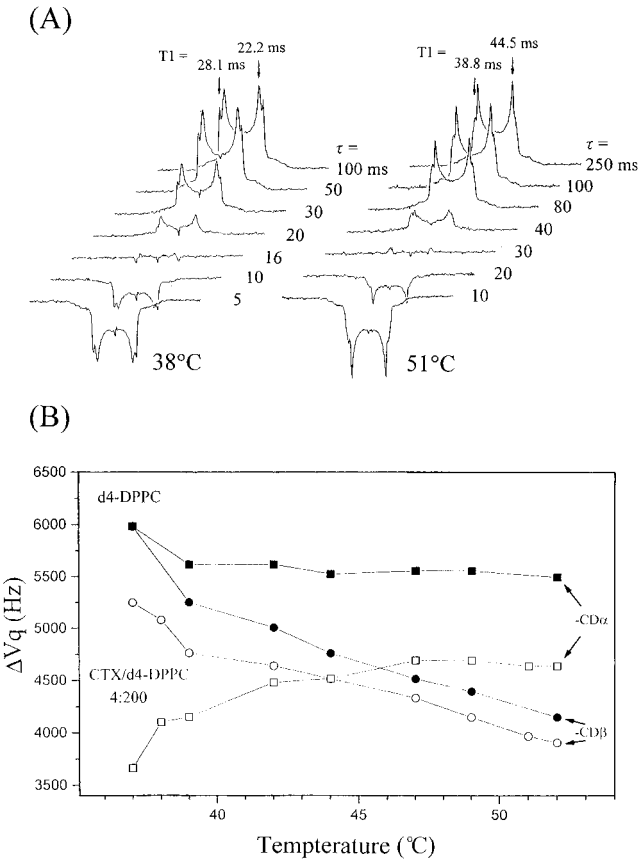

FIGURE 10: (A) Inversion recovery traces of the CTX/DPPC-d_4 complex at two different temperatures for the ^{2}H nucleus. (B) Variation of quadrupole splittings ($\Delta\nu_Q$) of the ^{2}H NMR signal obtained at C_α and C_β positions, as a function of temperature from the CTX/DPPC-d_4 complex. Molar concentration of CTX is 2/100. Filled symbols provide the same variation observed in the absence of CTX.

the liquid crystalline phase. In addition, since both values are also seen to be lower than that for pure DPPC-d_4, it indicates that both the conformation and the head group molecular order are significantly perturbed.

DISCUSSION

CTX is shown here to be capable of lysing DPPC membranes into smaller aggregates, presumably discoidal micelles, at the ripple phase. The optimum effective molar ratio of CTX to DPPC to carry out the complete lysing is estimated to be about 1/20, which shows that β-sheet CTX A3 is at least 2 times more potent than α-helical melittin of similar lytic activity. The quantitative difference between melittin and CTX can probably be attributed to the difference in the available hydrophobic surface area to fill up the exposed hydrophobic tail of the putative discoidal micelle formation, proposed previously by Dempsey (1990) for the melittin−PC membrane interaction. Assuming that the continuous hydrophobic region of CTX A3 is similar to that of CTX A5 (Sun et al., 1997), and that the hydrophobic residues of Leu-6, Val-7, Pro-8, Leu-9, Phe-10, and Tyr-11 from loop 1, Val-27, Ala-28, Pro-30, Lys-31, Val-32, Pro-33, Val-34, and Lys-35 from loop 2, and Leu-47, Leu-48, and Val-49 from loop 3 interact with the hydrophobic tail of PC micelles, the surface area covered by these amino acid residues is at least 2−3-fold larger than that for melittin.

The fusion of the CTX-induced small DPPC aggregates into an extended bilayer at T_m and the orientation of the aggregates in the magnetic field at the liquid crystalline state suggest a change in the CTX binding state, most likely a transition from a penetrating binding mode at the gel state to a peripheral binding mode at the liquid crystalline state (Dempsey, 1990). One of the simplest physical models to explain such a transition is the hydrophobic mismatch between the CTX and DPPC bilayer in the liquid crystalline state. The hydrophobic length of CTX is about 34 Å, which matches nicely with the dimension of the tilted fatty acyl chain of DPPC in the ripple phase, but this length appears to be too long for the bilayer hydrophobic thickness of about 25 Å in the liquid crystalline state of DPPC at which the CTX molecule is expelled from the transmembrane motif to the peripheral binding motif. This model is also consistent with the observation that the segmental order parameter of DPPC is respectively enhanced and decreased at temperatures just above and far above T_m.

CTX also influences the orientation and dynamics of the PC head group. Assuming that the effective charge of CTX A3 is the same as that of CTX A5 and the increase in membrane surface area upon CTX peripheral binding to POPC monolayers (Chiang et al., 1996) is about 400 Å^2, the effective charge of CTX A3 would be ∼2.2. Since the

orientation of the phosphocholine head group may act as a voltmeter near the membrane surface (Seelig et al., 1987), it is understood that the P−N dipole of the PC head group may tilt toward the water phase. The swing-back effect of the head group orientation of the CTX/DPPC complex at high temperature may be a result of weaker binding of CTX to DPPC bilayer at high temperature and/or a transition of the binding mode and thus the effective charge content, near the membrane surface. Although the details of the model are unclear, the significantly reduced molecular order of the PC head group in the CTX/DPPC complex clearly indicates that the interaction of the PC membrane with CTX is more complex than that with melittin. We have suggested recently that the head group arrangement of the phospholipid bilayer also plays a role in the protein−lipid interaction (Hsieh et al., 1997).

The notable absence of isotropic NMR signals only from the tail region in the ripple phase in conjunction with the rest of the spectroscopic data deserves further attention (Figure 8). The perturbing effect of CTX on the PC groups perhaps leads to a significant difference in the conformational and dynamic properties between the tail and head group regions. It is well known that if the principal axis of the tensorial interaction or the rotation axis of the nucleus makes an angle close to the magic angle 54.74° with the magnetic field then irrespective of the details of motion the interaction will be averaged to give an isotropic line in the NMR spectrum [see Sections 3.4 and 8.9 in Slichter (1991) and section 2.4 in Schmidt-Rohr and Spiess (1994)]. In the case of the lysed discoids in the ripple phase, all the methylene groups in the tail region are expected to be in the *trans* state where the angle subtended by the CD vectors with the axis of symmetry, namely, the acyl chain, is close to 90°, and in this phase the motional freedom for the lipid molecules within the bilayer is also restricted. Now these conditions show that the possibility for the methylene groups to get motionally averaged to give an isotropic NMR signal is rather limited. On the other hand if we assume that the angle subtended by the head group segment with respect to the bilayer normal is close to the magic angle (54.74°), then any motion of the lysed discoid as a whole can average the tensorial interaction to give an isotropic signal. The possibility of a specific orientation of the head group with respect to the magnetic field combined with the head group dynamics producing such an isotropic signal for the head group spectrum has been observed (Smith & Ekiel, 1984; Thayer & Kohler, 1981). In fact, the temperature dependent behavior of the quadrupole splittings of ^{2}H nuclei obtained specifically from the head group region supports the possibility of such a tilt of the head group. When the overall tumbling of the discoid is taken into consideration, it is not necessary that the angle subtended need be exactly equal to the magic angle. It should also be noted that such an averaging effect will be present, notwithstanding the restriction for motion for the lipid molecule within the bilayer. Nevertheless, we are not able to provide quantitative explanation on the aforementioned effect at this time.

Though the model presented in this paper for the CTX/DPPC interaction is qualitative, we feel that this seems to be the optimally consistent model right now explaining all the results presented here, and moreover it seems to clearly establish the penetration of β-sheet CTX into lipid bilayers. This study also shows that the binding mode of the P-type CTX A3 with zwitterionic PC is clearly different from that of the S-type CTX with negatively charged lipids. To put the model to further rigorous tests, a more versatile experimental technique like investigation of oriented bilayers with CTX is needed, and such work is currently underway in this laboratory. We have recently demonstrated that CTX binds to heparin and heparan sulfate specifically under physiological conditions and that the binding may potentiate the penetration of CTX into POPC monolayers (Patel et al., 1997). Analysis of the binding of CTX to heparin allowed us to identify a new β-sheet heparin-binding motif (Vyas et al., 1997). It would be interesting to perform an NMR study on the three-body interaction of CTX, heparin, and membrane bilayer. It would also be interesting to see if the binding of basic CTX to the acidic oligosaccharides near the cell surface affects the biological activity of the toxin either via the aforementioned tripartite interaction or via some unknown cell signaling pathway.

REFERENCES

Abe, T., Alema, S., & Miledi, R. (1977) *Eur. J. Biochem. 80*, 1−12.
Batenburg, A. M., & de Kruijff, B. (1988) *Biosci. Rep. 8*, 299−307.
Batenburg, A. M., Bougis, P. E., Rochat, H., Verkleij, A. J., & de Kruijff, B. (1985) *Biochemistry 24*, 7101−7110.
Bechinger, B. (1996) *J. Mol. Biol. 263*, 768−775.
Bilwes, A., Rees, B., Moras, D., Menez, R., & Menez, A. (1994) *J. Mol. Biol. 239*, 122−136.
Bloom, M., Davis, J. H., & Mackay, A. L. (1981) *Chem. Phys. Lett. 80*, 198−202.
Bougis, P., Rochat, H., Pieroni, G., & Verger, R. (1981) *Biochemistry 20*, 4915−4920.
Carbone, M. A., & Macdonald, P. M. (1996) *Biochemistry 35*, 3368−3378.
Chiang, C.-M., Chien, K.-Y., Lin, H.-J., Lin, J.-F., Yeh, H.-C., Ho, P.-L., & Wu, W. (1996) *Biochemistry 35*, 9167−9176.
Chien, K.-Y., Huang, W.-N., Jean, J. H., & Wu, W. (1991) *J. Biol. Chem. 266*, 3252−3259.
Chien, K.-Y., Chiang, C.-M., Hseu, Y.-C.,Vyas, A. A., Rule, G. S., & Wu, W. (1994) *J. Biol. Chem. 269*, 14473−14483.
Dauplais, M., Neumann, J. M., Pinkasfeld, S., Menez, A., & Roumestand, C. (1995) *Eur. J. Biochem. 230*, 213−220.
Davis, J. H. (1979) *Biophys. J. 27*, 339−358.
Dempsey, C. (1990) *Biochim. Biophys. Acta 1031*, 143−161.
Dempsey, C. E., & Watts, A. (1987) *Biochemistry 26*, 5803−5811.
Dempsey, C. E., & Sternberg, B. (1991) *Biochim. Biophys. Acta 1061*, 175−184.
Desormeaux, A., Laroche, G., Bougis, P. E., & Pezolet, M. (1992) *Biochemistry 31*, 12173−12182.
Dufourc, E. J., Smith, I. C. P., & Dufourcq, J. (1986) *Biochemistry 25*, 6448−6455.
Dufourcq, J., Faucon, J. F., Bernard, E., & Pezolet, M. (1982) *Toxicon 20*, 165−174.
He, K., Ludtke, S. J., Worcester, D. L., & Huang, H. W. (1996) *Biophys. J. 70*, 2659−2666.
Hsieh, C.-H., & Wu, W. (1996) *Biophys. J. 71*, 3278−3287.
Hsieh, C.-H., Sue, S.-C., Lyu, P.-C., & Wu, W. (1997) *Biophys. J. (in press)*.
Kuchinka, E., & Seelig, J. (1989) *Biochemistry 28*, 4216−4221.
Ludtke, S. L., He, K., Heller, W. T., Harroun, T. A., Yang, L., & Huang, H. W. (1996) *Biochemistry 35*, 13723−13728.
Macdonald, P. M., Leisen, J., & Marassi, F. M. (1991) *Biochemistry 30*, 3558−3566.
Mak, D.-O. D., & Webb, W. W. (1995) *Biochemistry 69*, 2323−2336.
Monette, M., Van Calsteren, M.-R., & Lafleur, M. (1993) *Biochim. Biophys. Acta 1149*, 319−328.
Pake, G. E. (1948) *J. Chem. Phys. 16*, 327−336.
Patel, H. V., Vyas, A. A., Vyas, K. A., Liu, Y.-S., Chiang, C.-M., Chi, L.-M., & Wu, W. (1997) *J. Biol. Chem. 272*, 1484−1492.
Picard, F., Pezolet, M., Bougis, P. E., & Auger, M. (1996) *Biophys. J. 70*, 1737−1744.

Pinheiro, T. J., Duralski, A. A., & Watts, A. (1994) *Biochemistry 33*, 4896−4902.
Pott, T., & Dufourc, E. J. (1995) *Biophys. J. 68*, 965−977.
Qiu, X., Mirau, P. A., & Pidgeon, C. (1993) *Biochim. Biophys. Acta 1147*, 59−72.
Roux, M., Neumann, J. M., Hodges, R. S., Devaux, P. F., & Bloom, M. (1989) *Biochemistry 28*, 2313−2321.
Salmon, A., Dodd, S. W., Williams, G. D., Beach, J. M., & Brown, M. F. (1987) *J. Am. Chem. Soc. 109*, 2600−2609.
Schindler, H., & Seelig, J. (1975) *Biochemistry 14*, 2283−2287.
Schmidt-Rohr, K., & Spiess, H. W. (1994) *Multidimensional solid-state NMR & Polymers*, Academic Press Inc., New York.
Seelig, A., & Seelig, J. (1974) *Biochemistry 13*, 4839−4845.
Seelig, J., Macdonald, P. M., & Scherer, P. G. (1987) *Biochemistry 26*, 7535−7541.
Slichter, C. P. (1991) *Principles of Magnetic Resonance, Third enlarged and updated edition*, Springer Verlag, Hong Kong.
Smith, I. C. P., & Ekiel, I. H. (1984) In *Phosphorous-31 NMR, Principles and Applications* (Gorenstein, D. G., Ed.) Chapter 15, Academic Press Inc., Orlando, FL.
Sternin, E., Bloom, M., & MacKay, A. L. (1983) *J. Magn. Reson. 55*, 274−282.
Sun, Y.-J., Wu, W., Chiang, C.-M., Hsin, A.-Y., & Hsiao, C-D. (1997) *Biochemistry 36*, 2403−2413.
Thayer, A. M., & Kohler, S. J. (1981) *Biochemistry 20*, 6831−6834.
Vyas, A. A., Pan, J.-J., Patel, H. V., Vyas, K. A., Chiang, C.-M., Sheu, Y.-C., Hwang, J.-K., & Wu, W. (1997) *J. Biol. Chem. 272*, 9661−9670.
Weaver, A. J., Kemple, M. D., Brauner, J. W., Mendelsohn, R., & Prendergast, F. G. (1992) *Biochemistry 31*, 1301−1313.
Wu, W. (1997) *Toxicology*: *Toxin Rev.* (submitted for publication).
Wu, W., & Huang, C.-H. (1983) *Biochemistry 22*, 5068−5073.

BI970413L